Cell

Structure and Organization of Coat Proteins in the COPII Cage

Stephan Fath,[1,2] Joseph D. Mancias,[1,2] Xiping Bi,[1] and Jonathan Goldberg[1,*]
[1] Howard Hughes Medical Institute and the Structural Biology Program, Memorial Sloan-Kettering Cancer Center, 1275 York Avenue, New York, NY 10021, USA
[2] These authors contributed equally to this work.
*Correspondence: jonathan@ximpact4.ski.mskcc.org
DOI 10.1016/j.cell.2007.05.036

SUMMARY

COPII-coated vesicles export newly synthesized proteins from the endoplasmic reticulum. The COPII coat consists of the Sec23/24-Sar1 complex that selects cargo and the Sec13/31 assembly unit that can polymerize into an octahedral cage and deform the membrane into a bud. Crystallographic analysis of the assembly unit reveals a 28 nm long rod comprising a central α-solenoid dimer capped by two β-propeller domains at each end. We construct a molecular model of the COPII cage by fitting Sec13/31 crystal structures into a recently determined electron microscopy density map. The vertex geometry involves four copies of the Sec31 β-propeller that converge through their axial ends; there is no interdigitation of assembly units of the kind seen in clathrin cages. We also propose that the assembly unit has a central hinge—an arrangement of interlocked α-solenoids—about which it can bend to adapt to cages of variable curvature.

INTRODUCTION

Vesicle transport pathways are responsible for the propagation and maintenance of organelles, and the underlying mechanisms of vesicle budding and fusion are conserved among eukaryotes (Bock et al., 2001). Budding occurs when cytoplasmic coat proteins assemble on a membrane surface, capture cargo molecules, and polymerize into spherical cages to bud off cargo-laden vesicles (Bonifacino and Glick, 2004; Kirchhausen, 2000). Cells contain a variety of coats—including COPI, COPII, and numerous clathrin/adaptor complexes—with each coat budding vesicles from a discrete subcellular location.

COPII-coated vesicles form on the endoplasmic reticulum (ER) to transport newly synthesized cargo to the Golgi complex. Three proteins—Sec23/24, Sec13/31, and the ARF-family GTPase Sar1—are sufficient to bud ~60-nm COPII vesicles from native ER membranes and from synthetic liposomes (Barlowe et al., 1994; Matsuoka et al., 1998). COPII budding is initiated by the activation of Sar1 to its GTP-bound form, causing it to translocate to the membrane and embed an N-terminal α helix in the bilayer (Antonny et al., 1997). Sar1-GTP recruits Sec23/24 to form a Sec23/24-Sar1 "prebudding complex" that binds directly to cargo molecules (Miller et al., 2003; Mossessova et al., 2003). The prebudding complex has a concave surface that conforms to the shape of the underlying membrane vesicle in order to maximize the opportunities for interactions with the membrane and with membrane-proximal elements of cargo proteins (Bi et al., 2002). Finally, the Sec13/31 complex is recruited through an interaction with Sec23/24, and it self-assembles into a polyhedron, leading to membrane deformation (Barlowe et al., 1994; Shaywitz et al., 1997; Stagg et al., 2006).

Electron microscopy (EM) studies of the isolated Sec13/31 assembly unit reveal a 28–30 nm rod, consistent in size with a heterotetramer composed of two Sec13 and two Sec31 polypeptides (Lederkremer et al., 2001; Matsuoka et al., 2001). Recently, the self-assembly reaction has been reconstituted using purified Sec13/31 protein, and the resultant cages have been analyzed by cryo-EM at 30 Å resolution (Stagg et al., 2006). This reveals a striking cuboctahedral architecture for the COPII lattice, built from 24 copies of the Sec13/31 assembly unit. The assembly unit constitutes the edge of the cuboctahedron, and four assembly units converge to form each of 12 vertices (Stagg et al., 2006).

The organization of the COPII cuboctahedron contrasts with that of clathrin cages, which remain the best-characterized vesicular carriers (Kirchhausen, 2000; Pearse et al., 2000). The clathrin lattice is built from triskelion assembly units—trimers of clathrin heavy chain—that are centered on the vertices of the cage, and the 47 nm long "legs" of the clathrin heavy chain interdigitate extensively with neighboring legs as they extend toward the adjacent vertices (Fotin et al., 2004b). Thus, both the symmetry and the nature of the vertex contacts seem to be completely distinct in clathrin and COPII lattices, but the relationship between these vesicular cages remains unknown in the absence of a molecular model of the COPII cuboctahedron.

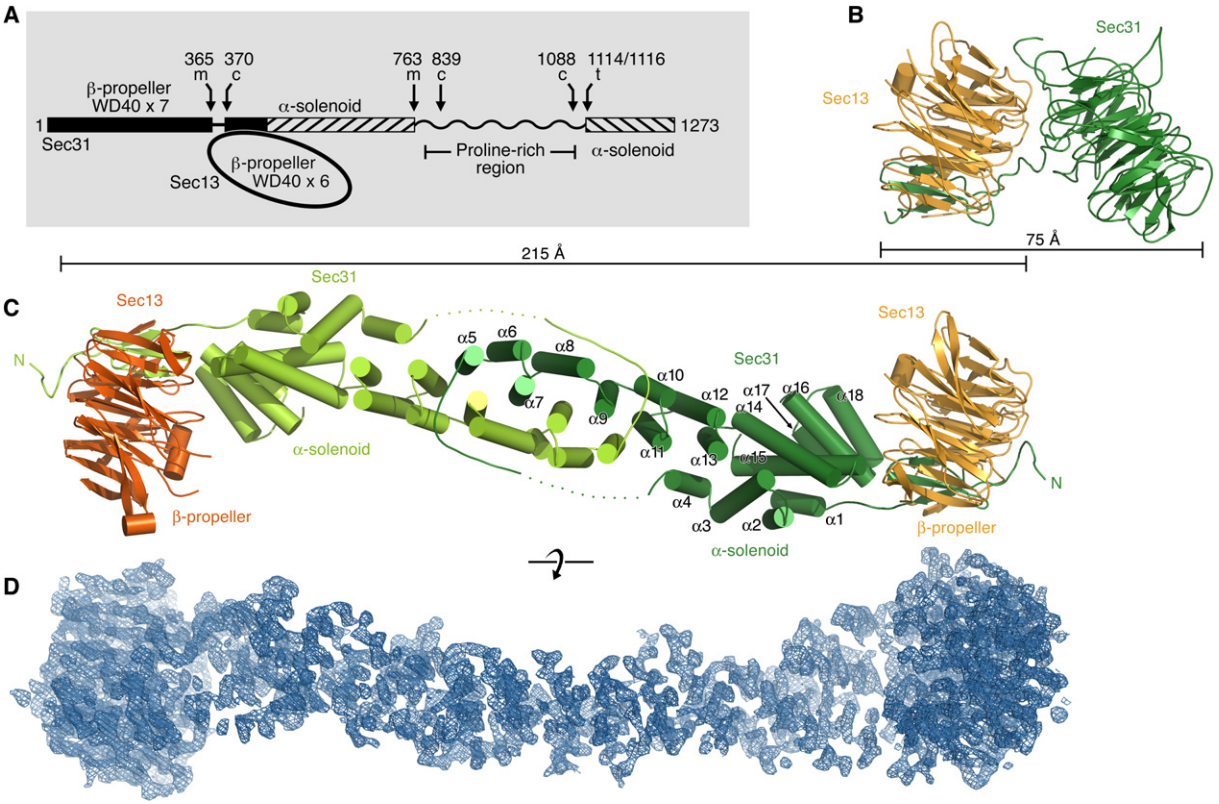

Figure 1. Structural Analysis of the Sec13/31 Complex

(A) Diagram shows the domain structure of *S. cerevisiae* Sec13/31 as defined by proteolytic mapping (see also Dokudovskaya et al., 2006). The products of limit proteolysis reactions were separated chromatographically, and discrete domains were sequenced to identify N termini (c, product of chymotrypsin cleavage; t, trypsin cleavage) and C termini (m, site determined by mass spectrometry measurement of the upstream domain).

(B) Ribbon representation of the Sec13/31 vertex element; the structure was determined by molecular replacement and refined to 3.3 Å resolution. The complex comprises full-length Sec13 colored orange and residues 1–411 of Sec31 colored green (corresponding to the N-terminal region colored black in [A]). β strands are drawn as arrows and α helices as cylinders.

(C) Ribbon diagram of the Sec13/31 edge element; the crystal structure was determined by MAD/SAD phasing and refined to 2.35 Å resolution. This complex comprises full-length Sec13 (red and orange) and the central α-solenoid domain of Sec31 (light and dark green) and forms a Sec13/Sec31-Sec31/Sec13 heterotetramer. The structure is viewed along the molecular dyad axis, oriented as in (B).

(D) Experimental electron density map (2.9 Å resolution, contoured at 2.0 σ) of the crystal asymmetric unit of the edge element, calculated using the combined MAD and SAD phases following density modification. View is rotated 90° from (C).

In this paper, we describe the atomic structure of the Sec13/31 assembly unit, and we present a molecular model of the COPII cage built by fitting the Sec13/31 crystal structures into the cryo-EM density map. We define the geometry of the multivalent contacts between assembly units at the cage vertices, the organizing principle for propagating the COPII cuboctahedron, and we compare the fundamentally different architectures of COPII and clathrin lattices.

RESULTS AND DISCUSSION

Domain Structure of Sec13/31

We prepared the yeast Sec13/31 complex by coexpression in baculovirus-infected insect cells and subjected the purified protein to limit proteolysis (Figure 1A; see also Dokudovskaya et al., 2006). Three protease-resistant products were obtained: the N-terminal β-propeller domain of Sec31 formed from seven WD40 sequence repeats or blades; the short C-terminal α-solenoid region of Sec31; and a complex comprising the central α-solenoid region of Sec31 (residues 370–763) and full-length Sec13, a β-propeller protein containing six WD40 repeats.

Absent from the proteolysis products was a stable portion of the proline-rich region, the domain of Sec31 that interacts with Sec23/24 (Shaywitz et al., 1997; Shugrue et al., 1999). Although transiently stable fragments were observed in some proteolysis reactions, we could not identify a robustly stable core, and we tentatively conclude that the proline-rich region is unstructured within the assembly unit (Figure 1A; 20% of residues 770–1110 are proline). Since this implies that the C-terminal α-solenoid domain of Sec31 may be flexibly linked to the remainder of the Sec13/31 complex, we tested whether this domain

Table 1. Data Collection and Refinement Statistics

Sec13/31 Complex		Edge		Edge	Edge	Vertex element
Data Set		MAD		SAD	Native	Native
PDB Accession #				2PM7	2PM6	2PM9
Space Group:		$P2_1$		$P2_1$	$P2_1$	$P4_3$
Cell Parameters a, b, c (Å) β (°)		128.1, 53.2, 133.1 108.4		128.2, 52.5, 133.1 108.3	128.4, 52.3, 133.1 108.6	155.2, 155.2, 59.9
Data Processing	Peak	Inflection	Remote	Peak		
Wavelength (Å)	0.9795	0.9798	0.9643	0.9795	1.54	0.9792
Resolution (Å)	50–2.8	50–2.8	50–2.8	40–2.35	30–2.45	40–3.3
R_{merge} (%)[a]	6.2 (29.0)[e]	5.7 (31.8)	6.3 (40.2)	4.7 (24.7)	4.1 (36.8)	9.2 (41.8)
I/σ	25.8 (5.1)	25.3 (4.4)	23.0 (3.4)	26.7 (4.6)	20.0 (2.4)	14.8 (2.1)
Completeness (%)	99.6 (99.9)	99.7 (99.6)	99.8 (99.4)	97.1 (91.1)	94.7 (93.2)	92.6 (76.3)
Redundancy	3.6 (3.7)	3.7 (3.6)	3.7 (3.6)	3.4 (3.2)	2.3 (2.2)	2.7 (2.2)
Refinement Statistics						
Data Range (Å)				30–2.35	30–2.5	40–3.3
Reflections				68541	54986	18996
Nonhydrogen Atoms				9938	9938	5170
Water Molecules				261	261	28
R.m.s. Δ Bonds (Å)[b]				0.006	0.007	0.008
R.m.s. Δ Angles (°)[b]				1.2	1.3	1.6
R Factor (%)[c]				24.2	25.2	25.1
R_{free} (%)[c,d]				29.8	30.1	30.5

[a] $R_{merge} = 100 \times \sum_h \sum_i | I_i(h) - \langle I(h) \rangle | / \sum_h \langle I(h) \rangle$, where $I_i(h)$ is the ith measurement and $\langle I(h) \rangle$ is the weighted mean of all measurement of $I(h)$ for Miller indices h.
[b] Root-mean-squared deviation (rms Δ) from target geometries.
[c] R factor = $100 \times \sum |F_P - F_{P(calc)}| / \sum F_P$.
[d] R_{free} was calculated with 5% of the data.
[e] Highest resolution shell is shown in parentheses.

might fold back to interact with the N-terminal regions, using a protein pull-down assay. We detected no interactions between the C-terminal α-solenoid domain and the β-propeller or central α-solenoid domains of Sec31 or with Sec13; nor did we detect evidence for self-association or interaction with the Sec23/24-Sar1 complex (data not shown).

This preliminary analysis suggested that the C-terminal portion of Sec31, encompassing the proline-rich region and terminal α-solenoid domain (residues 764–1273), might lie outside the "architectural core" of the assembly unit. Indeed, the crystallographic analysis described below confirms that the 28 nm long core particle is a Sec13/31-Sec31/Sec13 heterotetramer constructed from Sec13 plus the N-terminal region of Sec31 (the β-propeller and central α-solenoid domains).

Crystal Structure Determination

The atomic model of the assembly unit was built from two crystal structures of yeast Sec13/31 subcomplexes that we refer to as the edge and vertex elements (Table 1). Crystals of the edge element, comprising full-length Sec13 β-propeller and residues 370–763 (central α-solenoid) of Sec31, grew in space group $P2_1$ and contain a Sec13/31–Sec31/Sec13 heterotetramer in the asymmetric unit (Figure 1C). The initial electron density map was calculated to 2.9 Å resolution using combined phases from multi- and single-wavelength anomalous diffraction (MAD and SAD) experiments with selenium as the anomalous scatterer (Figure 1D shows the density-modified map). The structure of the edge element was refined to 2.35 Å resolution (Table 1). In order to facilitate this structure determination we mutated multiple conserved leucine residues to methionine (see Experimental Procedures). For completeness, we crystallized and refined a structure of the native protein to 2.45 Å resolution (Table 1). There are no significant conformational differences between selenomethionine mutant and native structures.

The crystal structure of the vertex element, comprising full-length Sec13 β-propeller and residues 1–411 (the β-propeller) of Sec31, was determined by the molecular replacement method using Sec13 as the search model

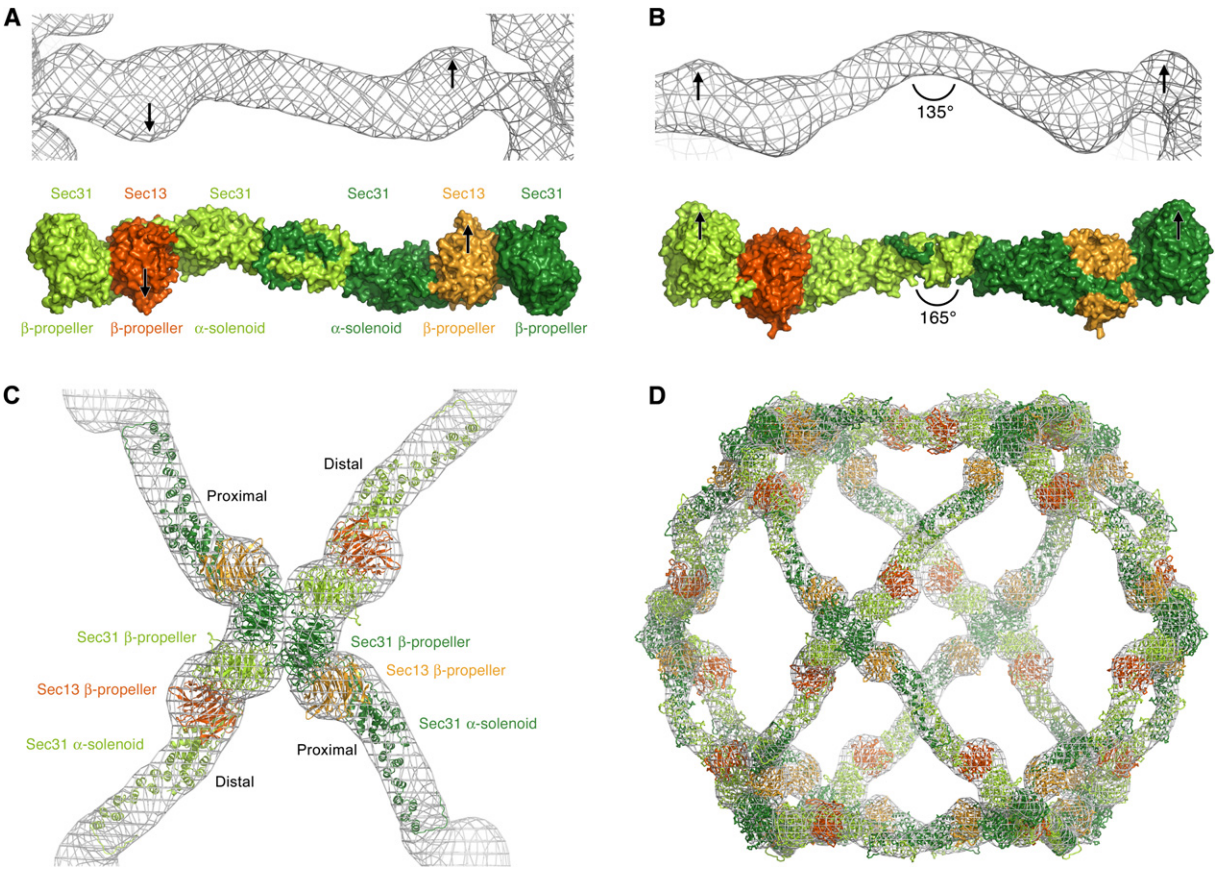

Figure 2. Organization of the Assembly Unit in the COPII Cage

(A) Comparison of the molecular model of the Sec13/31 assembly unit with the asymmetric unit of the cryo-EM map of the mammalian COPII cage (Stagg et al., 2006). The objects are viewed along the local 2-fold rotation axis. The model, shown in space-filling representation, is a composite of the two crystal structures (oriented and colored as in Figures 1B and 1C). The arrows indicate the ~15 Å displacement of the Sec13 β-propellers from the axis of the α-solenoid rod and the corresponding features in the cryo-EM map.

(B) Orthogonal view shows the difference in the angle at the center of the assembly unit. Here, the arrows show the 15–20 Å displacement of the Sec31 β-propellers from the α-solenoid axis.

(C) The molecular model of the heterotetrameric assembly unit was separated into two Sec13/31 heterodimers, and these were fitted independently as rigid bodies into the cryo-EM map (see Experimental Procedures). The picture shows a complete vertex (two asymmetric units of the cage) and is viewed along the 2-fold symmetry axis that runs through the vertex. One symmetry-related pair (colored dark green and orange) converges at the vertex and is labeled proximal; the other symmetry-related pair (light green and red) is labeled distal.

(D) The molecular model of the cage comprises 24 copies of the assembly unit with octahedral or 432 symmetry. Superimposed is the 30 Å cryo-EM density map from Stagg et al. (2006).

and refined with data to 3.3 Å resolution (Figure 1B). The polypeptide tracing was assisted by the regular arrangement of bulky tryptophan (or phenylalanine) residues of the WD signature on the A- and C-strands of the Sec31 β-propeller domain (Figure S1).

The crystal structures share a full-length Sec13 β-propeller, and, since this domain shows negligible conformational differences in the two crystal forms, it was possible to combine the structures straightforwardly to construct a composite model for the assembly unit, the 28 nm long Sec13/31-Sec31/Sec13 heterotetramer (Figures 2A and 2B).

Structure of the Assembly Unit

The structure of the COPII assembly unit comprises a central α-solenoid dimer capped by two β-propeller domains at each end (Figures 1B, 1C, 2A, and 2B). The α-solenoid regions of the two Sec31 molecules interact about a 2-fold symmetry axis to form a 14 nm long central rod (Figure 1C). The rod is relatively straight and is uniformly ~30 Å in diameter since it is formed from two α-solenoids along its length. However, the two Sec31 molecules are not arranged as an extended antiparallel dimer; instead each Sec31 polypeptide folds back on itself, creating an interlocked dimer. Helices α1–α4 fold back to form intermolecular interactions with helices α11–α18, and helices α5–α10 form isologous interactions with the opposite Sec31 molecule (Figure 1C).

The 28 nm long assembly unit is not uniformly straight along its length because the Sec31 and Sec13 β-propellers are displaced from the axis of the α-solenoid

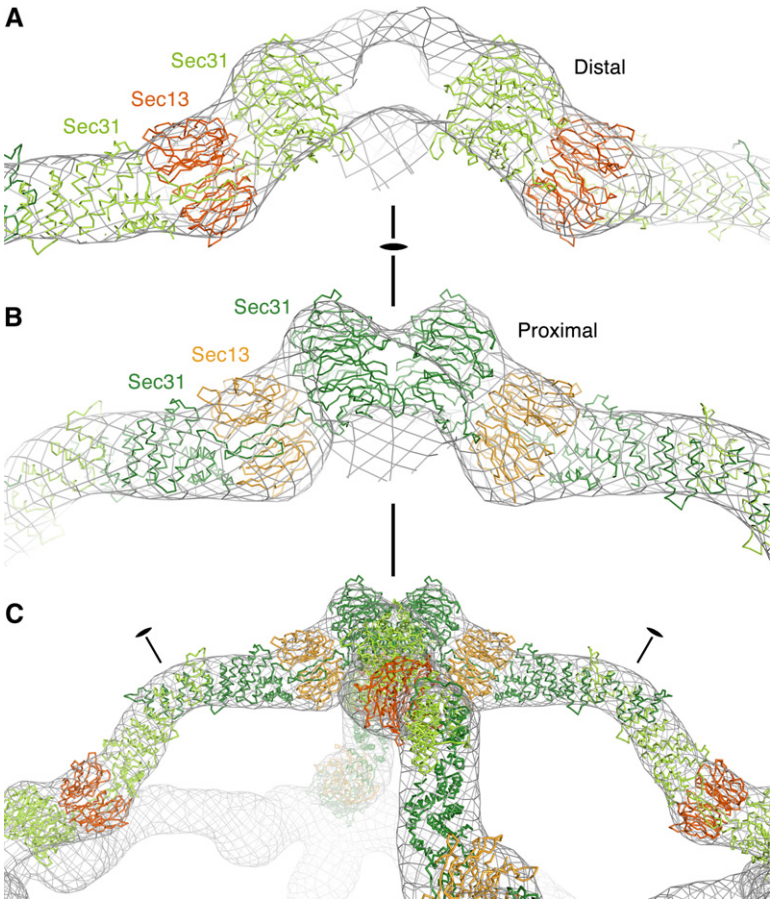

Figure 3. Fit of the Molecular Model to the Cryo-EM Map

(A) The distal pair. The picture shows the symmetry-related pair of ends of the assembly unit that are distal to the vertex dyad axis (vertical black line); the proximal ends are omitted. Superimposed is an ~40 Å section through the cryo-EM map (Stagg et al., 2006). This particular fit of model to cryo-EM map was optimized by reciprocal-space refinement (map correlation coefficient is 0.85; see Experimental Procedures). Note in (A) and (B) the fit of the Sec13 (red/orange) and Sec31 (light/dark green) β-propeller domains to features in the cryo-EM density map.

(B) The proximal pair. The view is rotated 90° about the vertical axis relative to (A), and the distal ends are omitted. Note the depression in the map at the vertex center that suggests a slight cant of the proximal Sec31 β-propellers.

(C) The picture is oriented as in (B) and shows four assembly units that converge at a vertex. The angled black lines indicate the local dyad axes of the assembly units (local means that the symmetry operators do not belong to the 432 point group of the cuboctahedron). Note the fit of the ~30 Å diameter solenoid rod to the tube of cryo-EM density.

rod (Figures 2A and 2B). Specifically, the Sec13 (inner) β-propellers are displaced ~15 Å from the α-solenoid axis, as can be seen most clearly in Figure 2A. Likewise, the Sec31 (outer) β-propellers are displaced 15–20 Å in a direction roughly parallel with the 2-fold axis of the assembly unit (Figure 2B). The off-axis arrangement of the Sec13 and Sec31 β-propeller domains gives the assembly unit its characteristic shape that can be recognized in the cryo-EM density map (Figures 2 and 3).

As the crystallographic results indicate, the Sec31 β-propeller domain is positioned at the ends of the assembly unit to mediate the vertex contacts that propagate the COPII cage (Figures 1–4). This is surprising from a structural perspective, as it means that the Sec13 molecule separates the β-propeller and α-solenoid domains of Sec31. Figures 4B and 4C show how the Sec31 polypeptide passes directly through Sec13 and contributes a seventh blade (Sec31 residues 380–406) to the six blades of the Sec13 β-propeller. This intimate interaction between the polypeptide chains is reinforced by extensive interfaces involving both axial ends of the Sec13 β-propeller: one end of Sec13 interacts with the Sec31 β-propeller (Figure S2); the other end interacts with the Sec31 α-solenoid domain (via the α14–α15 and α16–α17 loops plus helix α18 of Sec31; see Figure 1C). As a result, the β-propellers probably maintain a fixed orientation relative to the α-solenoid rod. This is important because it determines the geometry and hence the contact interfaces through which the Sec31 β-propellers converge at the vertex.

Fitting Sec13/31 into the Cryo-EM Density Map

The dimensions of the composite model of the Sec13/31 heterotetramer (Figures 2A and 2B) are consistent with images of the isolated assembly unit obtained in two EM studies, one of which employed negative staining and the other rotary shadowing to visualize COPII proteins (Lederkremer et al., 2001; Matsuoka et al., 2001). However, both studies revealed a range of conformations for the assembly unit in EM images that involved variation in the angle between the terminal domains and the center of the rod. In both studies it was inferred that the 28 nm long rod may be flexible about a central "protein hinge" (Lederkremer et al., 2001; Matsuoka et al., 2001).

The comparison of the molecular structure and the cryo-EM map of Stagg et al. (2006) provide additional evidence for a hinge located at the interlocked α-solenoid center of the rod (Figures 2A and 2B). When viewed along the 2-fold axis, the overall shape of the molecular model corresponds closely to the asymmetric unit of the cuboctahedron (Figure 2A). However, the orthogonal view (Figure 2B) reveals a major difference between the two structures: in the cryo-EM map, the two halves (two Sec31 molecules)

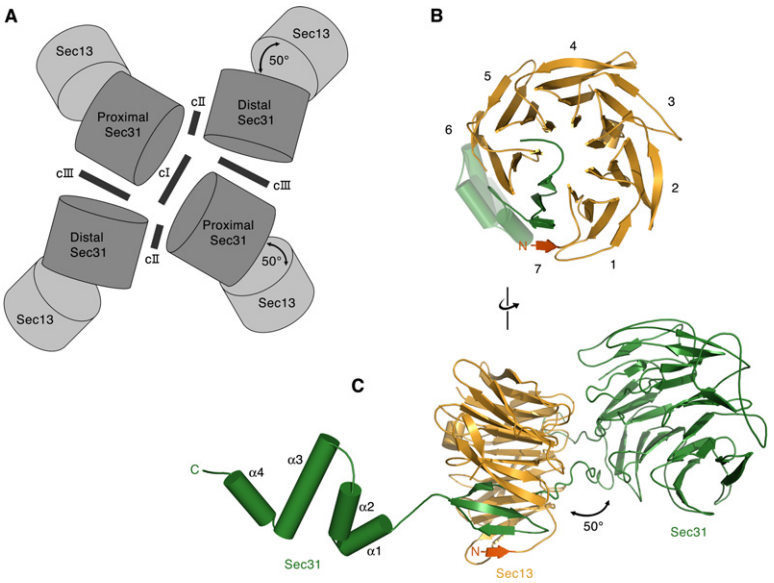

Figure 4. β-Propeller Folds and Vertex Geometry

(A) Schematic diagram of the vertex which forms from the convergence of four Sec31 β-propeller domains at the dyad symmetry axis. The diagram is based on the orientation shown in Figure 2C. Five contact interfaces are indicated with thick lines and are labeled: cI (involving proximal-proximal contacts), and cII and cIII (symmetry-related pairs involving proximal-distal contacts). The Sec13 β-propeller domains appear not to be involved in vertex contacts according to our model of the cage. The 50° angle between the axes of the Sec13 and Sec31 β-propellers is indicated (derived from the crystal structure of the vertex element).

(B) Ribbon diagram of the six-bladed Sec13 β-propeller (colored orange) emphasizing the seventh blade contributed by Sec31 (green). For clarity, the Sec31 β-propeller is omitted and only four helices of the α-solenoid are drawn in the background.

(C) Orthogonal view with the Sec31 β-propeller included. The 50° angle between the axes of the Sec13 and Sec31 β-propellers is indicated.

of the α-solenoid rod are bent 45° from parallel about the center of the rod, whereas in the crystal structure the angle is just 15°. This evidence for a hinge, together with the earlier EM analyses, suggests a mechanism by which the Sec13/31 assembly unit could adapt to lattices of variable curvature, as discussed in more detail below. (Hinge is not meant to imply that the α-solenoid interface is disordered in the crystal structure of the edge element; this region is in fact well ordered with lower crystallographic B-factors than the average for the molecule; Figure S3).

For fitting into the cryo-EM map, we separated the molecular model of the assembly unit into two halves (at the α-solenoid interface) and fitted these independently as rigid bodies into the 30 Å map (Figures 2C and 2D). Initial fitting was done manually and then improved via real- and reciprocal-space approaches, which gave essentially the same result from a range of refinement starting points (see Experimental Procedures). The complete molecular model of the COPII cage, comprising 24 copies of the assembly unit with octahedral symmetry, is illustrated in Figure 2D. The quality of the fit is indicated in Figure 3, which shows the correspondence of the Sec13 and Sec31 β-propellers to features in the cryo-EM map (the map correlation coefficient for the fit shown in Figures 2 and 3 is 0.85). We did not attempt to model in detail the hinge region at the interlocked Sec31-Sec31 center owing to the low resolution of the cryo-EM data.

Vertex Geometry and Molecular Model for the COPII Cage

The Sec13/31-Sec31/Sec13 assembly unit constitutes the asymmetric unit of the COPII cuboctahedron (Stagg et al., 2006). This means that although the assembly unit is a symmetric dimer, it is utilized as an asymmetric rod to construct the cage (in other words, the 2-fold symmetry operator of the assembly unit does not belong to the 432 point group of the cage). Importantly, this also means that the two ends of the assembly unit are in different environments at the cage vertices. At one end, a Sec31 β-propeller converges at the vertex dyad axis and interacts with its β-propeller symmetry partner—we refer to this as the proximal Sec31 β-propeller (Figures 2C, 3, and 4A). At the other end of the assembly unit, the distal β-propeller resides ~20 Å from the vertex dyad axis and does not interact with its symmetry partner.

As this description implies, the vertex is constructed from four Sec31 β-propellers: a proximal pair and a distal pair. Figure 3 illustrates the excellent fit of the proximal and distal β-propellers to the cryo-EM density. Since both ends of the assembly unit were fitted into the map as rigid bodies, this suggests that the disposition of the α-solenoid and β-propeller domains is essentially the same at the proximal and distal ends. We surmise that flexibility is limited to the interlocked α-solenoid center of the rod and that plasticity at the β-propeller interdomain contacts is not required for the optimal positioning of the proximal and distal ends in their distinct environments at the vertex. This proposal is substantiated by the aforementioned extensive interfaces between the β-propeller and α-solenoid domains.

When viewed along its 2-fold axis, as in Figure 2C, the vertex can be described as a distorted 4-fold center such that the proximal and distal β-propellers converge on the vertex in a similar orientation. As a consequence, all four Sec31 β-propellers are positioned with their flat axial ends mediating the major contact interfaces (Figure 4A). This geometry is imposed by the relative juxtaposition of the β-propeller and α-solenoid domains along the rod. Specifically, the axis of the Sec13 β-propeller is parallel with, and displaced ~15 Å from, the α-solenoid axis; the

Sec31 β-propeller axis in turn is inclined at a 50° angle to the Sec13 β-propeller axis (Figure 4).

Figure 4A illustrates the relationship between the pairs of proximal and distal Sec31 β-propellers. The assembly unit is pentavalent, forming three contact interfaces via its proximal end (labeled cI, cII, and cIII in Figure 4A) and two at the distal end (cII and cIII). Thus the molecular model of the cage comprises 24 pentavalent assembly units that form 12 vertices. The multivalent nature of the vertex interactions is the principle for organizing a tetramer at the vertex, and the individual pairwise contacts (cI, cII, and cIII) and the assembly-unit dimers that correspond to them are likely to be exceedingly weak. The cI proximal-proximal contact appears not to involve the entire surface of the axial end of the Sec31 β-propeller because the β-propeller is tilted ~13° from the vertex 2-fold axis. This slight cant of the proximal β-propellers is suggested by a depression in the cryo-EM map at the vertex center (Figure 3B). We have not explored other features of the vertex contacts in atomic detail at this stage because the current cryo-EM data provide for a relatively low-resolution model of the cage.

For descriptive purposes we referred to the vertex as a distorted 4-fold center. In reality the distal β-propellers are translated ~15 Å in toward the center of the cage relative to the proximal β-propellers (Figure 3C). Thus, the cIII proximal-distal interface joins two Sec31 β-propellers that are related by an ~90° rotation and an ~15 Å translation (Figure 4A). A similar interaction to cIII is observed as a crystal contact in the crystals of the vertex element, where it propagates the 4_3 crystallographic screw axis (c = 59.9 Å). Our model predicts that the vertex element illustrated in Figure 1B should form a tetramer in solution at sufficiently high concentrations. However, we detected only monomeric Sec13/31(1–411) in gel filtration experiments using protein concentrations up to 30 mg/ml (data not shown). We propose that in the COPII polyhedron, as in viral capsids, the ligation of multiple very weak vertex contacts yields a globally stable cage. Weak vertex interactions are presumably important in the self-assembly reaction to prevent the accumulation of too many nuclei—we assume that Sec13/31 nucleation involves the low-probability association of four assembly units to form a vertex. The other general possibility in this context is that assembly is assisted by a template protein—an assembly chaperone—though there is no evidence for such a factor in COPII coat formation.

In summary, the positions of the β-propeller and α-solenoid domains in the COPII cage have been assigned unambiguously to structural features of the 30 Å cryo-EM map. Although the details of the vertex contacts in our model of the cage cannot be assessed at this resolution, it is nevertheless clear that the pairwise contacts of the Sec31 β-propellers look much like conventional protein-protein interactions and that the vertex is not constructed through the interdigitation of assembly units. Thus, both the symmetry and nature of the vertex contacts are completely distinct in COPII and clathrin cages.

Finally, Stagg et al. (2006) observed that the 2-fold symmetry axis of the assembly unit is not located centrally along the edge of the cuboctahedron. Consistent with this, we find that the 30 Å diameter central α-solenoid dimer fits well into the cryo-EM map and the interlocked Sec31-Sec31 center coincides with the 2-fold symmetry center of the assembly unit in the map (Figures 2 and 3). Although the symmetry of the assembly unit is not connected to the symmetry of the cage, the assembly unit is oriented such that its 2-fold axis passes close to the center of the cuboctahedron (Figure 3C).

COPII and Clathrin Lattices

COPII and clathrin cages are both constructed from α-solenoid and β-propeller building blocks (Fotin et al., 2004b; ter Haar et al., 1998; Ybe et al., 1999). We observe a close correspondence of the COPII and clathrin α-solenoid folds despite some divergence at the point where the two Sec31 chains interlock (in the vicinity of helix α9; see Figure S4). In particular, both α-solenoids follow a straight path that is distinct from the highly curved forms observed in other α-solenoid structures (Kajava, 2002). (The α-solenoid fold is also termed α-helical zigzag; ter Haar et al., 1998.)

α-solenoid and β-propeller folds have also been identified through sequence analysis in COPI coat proteins and in the yNup84/vNup107–160 subassembly of the nuclear pore complex. On this basis it has been posited that a common ancestor of vesicle-coat and nuclear-pore complexes—a membrane-curving module—arose with the emergence of the endomembrane system to stabilize curved membranes (Devos et al., 2004). It is surprising then that the α-solenoid and β-propeller domains are arranged in such fundamentally different ways in COPII and clathrin such that they form distinct symmetry centers and assembly-unit interactions that propagate the cages. In clathrin, a triskelion assembly unit lies at each vertex, and the α-solenoid legs of neighboring triskelia interdigitate extensively as they extend toward the adjacent vertices; the β-propeller is not part of the architectural core and instead projects in toward membrane to interact with adaptor molecules (Fotin et al., 2004b; Kirchhausen, 2000). In contrast, the COPII assembly unit is a rod that constitutes the edge of a cuboctahedron, and four rods converge to form the vertex with no interdigitation of assembly units. α-solenoid domains form the core of the edge, but, unlike clathrin, the COPII vertices are formed from β-propellers. In summary, the COPII and clathrin lattices seem not to share common construction principles other than the use of α-solenoid and β-propeller folds. Future structural studies of the COPI cage and the nuclear pore complex should reveal whether common principles exist and will shed more light on the evolutionary relationships among these membrane-curving proteins.

A Possible Mechanism for Lattice Adaptability

The ability of COPII coat proteins to control ER exit of very large cargo molecules such as procollagen and

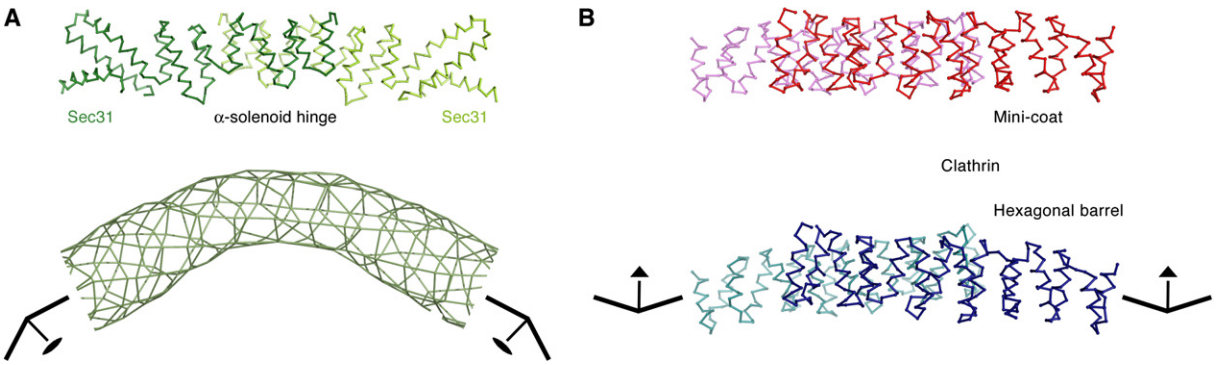

Figure 5. α-Solenoid Crossing Angle and a Possible Mechanism for Lattice Adaptability

(A) COPII. Comparison of the crystal structure with the cryo-EM map, focused on the crossing angle of the Sec31 α-solenoids. The Cα trace shows the dimerization region, with the Sec31 polypeptides colored light and dark green. (The molecular dyad axis is vertical). The corresponding view of the cryo-EM map suggests a 30° rotation between the two Sec31 α-solenoid rods relative to the crystal structure (also see Figure 2B). The symbols indicate the vertices with their dyad symmetry; the hinge is orientated such that a decrease in the hinge angle would yield a smaller cage, according to our model.

(B) Clathrin. Comparison of molecular models of the "proximal pair" of α-solenoids based on cryo-EM analysis of the clathrin mini-coat (top) and hexagonal barrel (bottom; Fotin et al., 2004b); the models differ by an 8° rotation. The vertices have 3-fold rotational symmetry, and the hinge is inverted relative to COPII such that a decrease in the hinge angle yields a larger cage. We do not mean to imply that the overlapped α-solenoids interact in a similar manner in COPII and clathrin; indeed, only the COPII α-solenoids form intimate contacts across the interface.

chylomicron raises the question of whether COPII vesicles larger than the standard 60 nm cages can form from lattices of altered curvature (Fromme and Schekman, 2005). Larger (>60 nm) cages have been identified in cryo-EM images of self-assembled Sec13/31 but have not as yet been analyzed in detail (Stagg et al., 2006). Lattice adaptability of this kind has been observed for clathrin, whereby cargo size can influence triskelion self-assembly and dictate the dimensions of the cage (Crowther et al., 1976; Fotin et al., 2004b; Heuser, 1980; Ehrlich et al., 2004). At the molecular level, a larger clathrin cage that incorporates additional assembly units requires changes in lattice contacts, and this is achieved through an alteration of the crossing angle between adjacent α-solenoids along the edge (Fotin et al., 2004b; Figure 5B). We propose that a similar mechanism may control the size of the COPII cage (Figure 5). That is, we envisage a larger COPII cage that incorporates additional assembly units (with additional polygonal facets) and a concomitant alteration of the crossing angle at the Sec31-Sec31 protein hinge. At the center of the assembly unit, the putative protein hinge involves two Sec31 α-solenoid chains that overlap to form a 50 Å long interface (Figures 1C and 5), an arrangement that resembles the overlapping clathrin proximal and distal α-solenoid pairs (though only the COPII α-solenoids form intimate contacts across the interface). If flexibility at the α-solenoid crossing angle compromises cage integrity, in clathrin this might be counteracted by the extensive interdigitation of triskelia, whereas in COPII the interlocked arrangement of Sec31 α-solenoid chains may be an important stabilizing factor (Figure 1C).

The notion that the Sec13/31 assembly unit is flexible about a central protein hinge was proposed based on two EM studies (Lederkremer et al., 2001; Matsuoka et al., 2001) and is reinforced by the observed difference in hinge angle between the X-ray structure and cryo-EM map (Stagg et al., 2006). The protein-hinge model and its relation to the clathrin system will be tested as cryo-EM analyses of the COPII cuboctahedron and larger cages are extended to higher resolution.

Functional Organization of the COPII Coat

The model in Figure 6 illustrates the arrangement of protein components and membrane in the COPII vesicle. Twenty-four copies of the 28 nm assembly unit organize themselves as a cuboctahedron with an outer diameter of ~60 nm and an inner diameter of ~52 nm (these are average measurements as different parts of the assembly unit reside at different radial distances). For comparison, COPII-coated vesicles synthesized in vitro from ER membranes measure 60–65 nm diameter and contain a 10 nm thick coat that is thought to comprise the ~5 nm cage or "outer layer" plus a 5 nm inner layer of multiple Sec23/24-Sar1 complexes (Barlowe et al., 1994; Lee et al., 2004; Matsuoka et al., 2001). On this basis we modeled the membrane vesicle as a 40 nm sphere, two-thirds of the diameter of the cage, to allow an ~5 nm space for Sec23/24-Sar1, two copies of which are drawn in Figure 6. This estimate of the vesicle diameter may be on the high side, as a recent study of clathrin-coated vesicles employing electron cryo-tomography of individual particles reveals somewhat smaller membrane vesicles, which are on average ≤50% of the diameter of the surrounding protein coat (Cheng et al., 2007).

The Sec13/31 cuboctahedron contains binding sites for 48 copies of the inner-layer Sec23/24-Sar1 complex (only two copies are drawn in Figure 6 for clarity). This assumes that the proline-rich region of Sec31, known to interact with

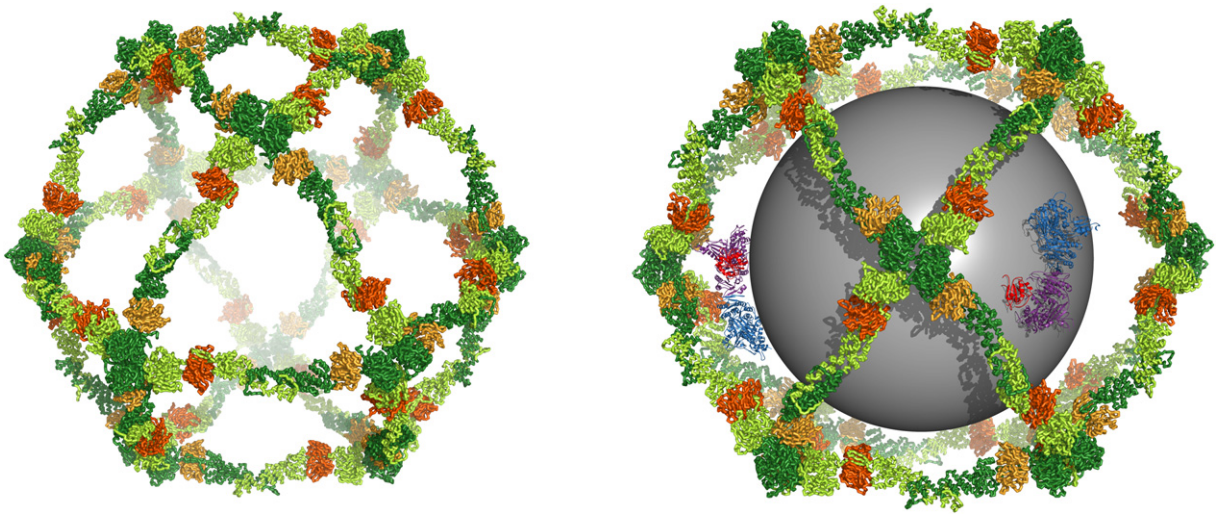

Figure 6. Molecular Model of the COPII Cage

The model of the cage is drawn as a backbone worm and colored as in Figures 1–3. The view on the left is approximately along the 3-fold symmetry axis of the cuboctahedron. The view on the right is along the vertex 2-fold axis. Modeled inside the cage is a sphere of diameter 40 nm representing a membrane vesicle. For comparison, the "inner diameter" of the cage is ~52 nm—this is the mean protein-to-protein measurement that passes through the center of the cage. The smallest such distance, measured close to the vertex, is ~49 nm. The mean outer diameter of the cage is ~60 nm, and the longest such measurement is ~63 nm. Also modeled are two copies of the Sec23/24-Sar1 prebudding complex, taken from Bi et al. (2002). Sec23 is colored magenta, Sec24 is blue, and Sar1 is red.

Sec23/24 (Shaywitz et al., 1997; Shugrue et al., 1999), is functionally accessible on the 24 proximal and 24 distal ends of the assembly unit (the 340 residue proline-rich region follows helix α18; see Figure 1C). Since the concave membrane-apposing surface area of Sec23/24-Sar1 measures ~8,200 Å^2 (Bi et al., 2002), 48 copies of the complex would cover 75%–80% of the surface area of a 40 nm vesicle. This could in principle leave sufficient space for the cytoplasmic regions of transmembrane cargo proteins—a quantitative analysis of the composition of synaptic vesicles shows that protein transmembrane domains comprise ~18% of the surface area of the outer leaflet (Takamori et al., 2006). However, it seems unlikely that the inner-layer complexes are this densely packed and more reasonable to assume that substoichiometric amounts of Sec23/24-Sar1 are incorporated into the COPII coat. Single-particle analysis of clathrin-coated vesicles shows that the inner layer is not as densely packed as would be predicted if AP2 adaptors (or their functional equivalents) were bound stoichiometrically to the clathrin heavy chain (Cheng et al., 2007). And this observation was interpreted in terms of a budding reaction in which the connection of clathrin assembly units to the membrane via inner-layer adaptors is required for the initiation, but not for the completion, of budding (Cheng et al., 2007).

The concept of a vesicular coat as a mechanical device for budding vesicles implies that the driving energy for self-assembly of the spherical cage—which arises from the compulsion to maximize the number of stable bonds between assembly units—is directly coupled to membrane deformation. In the case of the Sec13/31 cage, the connection to lipid membrane is through Sec23/24 to the N-terminal amphipathic α helix of the Sar1-GTP molecule (Barlowe et al., 1994; Shaywitz et al., 1997). According to the calculations above, as many as 48 (but probably fewer) copies of Sar1-GTP will provide the linkages by which the Sec13/31 assembly units incrementally deform the membrane into an ~40nm bud. Sar1-GTP may, in addition, play a direct role to initiate membrane curvature since it embeds its amphipathic α helix in the cytosolic leaflet of the membrane (Bielli et al., 2005; Lee et al., 2005). If we assume a unitary stoichiometry among the COPII components, then the amphipathic α helices of 30–48 copies of Sar1-GTP will displace an area of lipid that corresponds to 1.4%–2.4% (±0.4%) of the surface area of the outer leaflet of a 40 nm vesicle. Since the area of this outer leaflet is 55%–60% larger than the inner leaflet, the contribution of Sar1-GTP to membrane curvature is more likely to be catalytic than stoichiometric. Conceivably, supernumerary Sar1-GTP molecules incorporate into the bud to impart curvature, but it is unclear how these would be organized in the absence of a link to the other COPII coat components.

The molecular model of the Sec13/31 assembly unit constructed from the crystallographic analysis seems to account for all the density in the cryo-EM map (Figures 2D and 3). Thus, the architectural elements of the assembly unit comprise Sec13 plus the β-propeller and central α-solenoid domains (residues 1–763) of Sec31 (Figure 1A). The C-terminal region of Sec31 (residues 764–1273) is not part of the architectural core, and we infer that this region is not observed following image reconstruction from electron cryo-micrographs of multiple cages as it does not conform strictly to the symmetry of the cage (Stagg et al.,

2006). The 55K C-terminal region comprises the 35K proline-rich segment plus the terminal α-solenoid domain (Figure 1A). The low sequence complexity of the proline-rich segment and its sensitivity to proteolysis suggest that this region is largely unstructured and forms a flexible linker to the terminal α-solenoid and that the 55K region projects in toward the membrane to engage Sec23/24 (via a portion of the proline-rich segment; Shaywitz et al., 1997). A flexible connection between the Sec13/31 cage and the Sec23/24-Sar1 complex would afford Sec23/24-Sar1 some mobility on the membrane surface, perhaps facilitating the packaging of a variety of cargo proteins of different shapes and sizes.

Sec13/31 forms a more open lattice than clathrin due to the octahedral symmetry of the cage and the distinct composition of the cage edge. Regarding symmetry, the clathrin lattice forms a wide variety of designs of cages but in general seems to require about 60 edges to build a cage around a 40 nm vesicle (Cheng et al., 2007); by contrast the COPII cuboctahedron uses 24 edges to surround a vesicle of comparable size. Regarding the composition of the edge, in the clathrin cage these are composed of four α-solenoid chains, whereas the COPII cage edge involves just two α-solenoids (Fotin et al., 2004b). The net effect is to create an open COPII lattice: in particular, the square face of the cuboctahedron measures ~27 nm from side-to-side and ~33 nm across the diagonal (Figures 2D and 6). This may be large enough to accommodate the neck of the membrane bud, and if this is a stable arrangement it raises the question of whether the completion of cage assembly can in and of itself drive vesicle fission. Recent studies of yeast and mammalian COPII proteins suggest that cage formation is insufficient and reveal a major role for Sar1-GTP in the fission reaction, possibly involving the amphipathic α helix invading and constricting the bud neck (Antonny, 2006; Bielli et al., 2005; Lee et al., 2005).

Finally, the distinct organization of COPII and clathrin cages, in terms of symmetry and the interdigitation of assembly units, has implications for the disassembly reaction. The heavily interdigitated clathrin lattice requires hsc70 and the cochaperone auxilin to effect structural perturbations at the vertex that lead to global uncoating (Braell et al., 1984; Fotin et al., 2004a). Disassembly of the Sec13/31 lattice may be more straightforward since its stability relies on fewer vertices and on less extensive interactions between assembly units and there is no evidence that COPII uncoating is a regulated process.

EXPERIMENTAL PROCEDURES

Protein Production

The full-length and all truncated forms of yeast Sec13/31 were prepared by coexpression in insect cells infected with engineered baculoviruses (relative molecular mass of Sec13, 33K and Sec31, 139K). Sec31 forms were designed with an N-terminal His_6 tag. Insect cells were harvested 48 hr postinfection and lysed by sonication, and proteins were purified by Ni^{2+}-IMAC and ion-exchange (Q-Sepharose) chromatography. Histidine tags were removed with TEV protease (Invitrogen), followed by size-exclusion chromatography on a superdex 200 column. (The ion-exchange step was omitted for the vertex element.) Protein for crystallization experiments was concentrated and flash-frozen in liquid nitrogen. Full-length Sec13/31 was probed with trypsin and chymotrypsin, and the limit products were purified by ion-exchange chromatography and analyzed by N-terminal sequencing and mass spectrometry.

For selenomethionine incorporation, insect cells were incubated for 24 hr prior to viral infection at 1.5 million cells/ml in Met/Cys-free medium supplemented with 20 mg/l L-selenomethionine and 2 mM cysteine (medium A). At 5 hr postinfection, cells were pelleted and resuspended in medium A. Following 24 hr incubation, the selenomethionine concentration was increased to 80 mg/l and cells were harvested after a further 24 hr incubation. Protein was extracted from cell lysates as before. The extent of selenomethionine incorporation into the core Sec13/31 complex was ~75%, as assessed by mass spectrometry. To increase the selenomethionine content, we mutated six conserved leucine residues to methionine in Sec13 (residues 11, 17, 24, 80, 115, and 222) and made five such changes in Sec31 (residues 449, 536, 615, 622, and 674).

Crystallization and Structure Determination

The Sec13/31 edge complex (comprising full-length Sec13 and residues 370–763 of Sec31) was crystallized at 4°C by the hanging-drop method. To 1 μl of 35 mg/ml protein solution was added 1 μl of well solution containing 15% polyethylene glycol (PEG) 4000, 10% dimethylsulfoxide, 6% dioxane, and 100 mM Tris-HCl (pH 7.5). Hanging drops were seeded with microcrystals after two days equilibration. The crystals are monoclinic, space group $P2_1$ (a = 128.2 Å, b = 52.5 Å, c = 133.1 Å, β = 108.34), and contain $(Sec13/31)_2$ in the asymmetric unit. For diffraction studies, crystals were transferred to 15% PEG 4000, 25% dimethylsulfoxide, and 100 mM Tris-HCl (pH 7.9) and were flash-frozen in liquid propane.

The edge structure was determined via MAD and SAD experiments. SAD data were collected from a single frozen crystal at beamline X25 of the National Synchrotron Light Source (NSLS). Data were processed with the program HKL2000 (Otwinowski and Minor, 1997), and SAD analysis was done with the program SOLVE (Terwilliger and Berendzen, 1999) using data between 38 and 2.6 Å resolution. Solve found 20 of the 30 selenium atom positions and, following refinement, reported a mean figure of merit (fom) of 0.31. MAD data at three wavelengths from 38 to 2.9 Å resolution were collected (also at beamline X25), and analysis with SOLVE gave a fom of 0.44. The MAD and SAD phases were combined using SIGMAA (CCP4, 1994) to give a fom of 0.55 for data between 38 and 2.9 Å resolution. Density modification with noncrystallographic symmetry averaging was carried out with DM (CCP4, 1994), yielding an initial electron density map of high quality. Model refinement using the program CNS (Brünger, 1998) reduced the R factor to a final value of 24.2% (R_{free} of 29.8%) for data (from the SAD experiment) between 30.0 and 2.35 Å resolution. The model comprises 9938 protein atoms and 261 water molecules, with just three Ramachandran violations (residue 146 in both copies of Sec13 and residue 497 in one copy of Sec31). Finally, native data from 30 to 2.5 Å resolution were collected on a rotating anode X-ray generator and used to refine a model of the native protein (final R factor = 25.2; R_{free} = 30.3). In the models (SAD and native), the following residues been omitted due to weak electron density: 370–372, 470–494, 691–693, and 746–763 in Sec31 and residues 1, 158–169, and 292–297 in Sec13. The X-ray data and refinement statistics are summarized in Table 1.

Crystals of the Sec13/31 vertex element were formed at 22°C by the hanging-drop method. This complex comprises residues 1–411 of Sec31 plus full-length Sec13 that contains the six Leu-to-Met mutations described above. Hanging drops containing 15 mg/ml protein, 8% PEG 3350, and 100 mM trisodium citrate, and 10 mM manganese (II) chloride were equilibrated over well solutions of 16% PEG 3350 plus 200 mM trisodium citrate. The crystals (space group $P4_3$, a = 155.2 Å,

c = 59.9 Å, 75% solvent) contain one vertex element in the asymmetric unit. For diffraction experiments crystals were transferred to well solution containing an additional 25% glycerol and were flash-frozen in liquid propane. X-ray data were collected at beamline 24ID of the Advanced Photon Source (APS) and processed as before. The structure was solved by molecular replacement with the program AMORE (CCP4, 1994) using Sec13 as the search model. Initial electron density was markedly improved using the prime-and-switch function of the program RESOLVE (Terwilliger and Berendzen, 1999), and the complete Sec13/31 vertex element was built iteratively with rounds of refinement using CNS (Brünger, 1998). The final R factor is 25.1% (R_{free} of 30.5%) for data between 40.0 and 3.3 Å resolution (Table 1). There are two outliers in a Ramachandran plot of the final model (Ser156 and Phe369 of Sec31). The following residues have been omitted due to weak electron density: Sec13 residues 1, 158–168, and 293–297 and Sec31 residues 1–4 and 411.

Fitting into the Cryo-EM Density Map

The atomic model of the assembly unit (that is, the composite of the two crystal structures) was separated (at the Sec31-Sec31 dimer interface) into two halves, and these were fitted independently as rigid bodies into the 30 Å cryo-EM map determined by Stagg et al. (2006). Initial fitting was done manually using O (Jones et al., 1991) and was improved via real- and reciprocal-space approaches. For real-space optimization, electron density maps for each half of the atomic model were calculated to the nominal resolution of the cryo-EM map and then fitted to the cryo-EM map using MAVE (and related programs from the Uppsala suite; Kleywegt and Jones, 1999).

Alternatively, the initial fit was improved by reciprocal-space refinement of the two rigid bodies using CNS (Brünger, 1998), having first transformed the cryo-EM map. We imposed a very soft van der Waals penalty on intermolecular (432 symmetry-related) contacts in CNS to restrict overlap of Sec31 β-propellers at the vertex. This energy term was not enforced at the α-solenoid crossover site, and no attempt was made to model the hinge region, as the resolution limit of the cryo-EM data is insufficient for this at present.

The fit used for the illustrations (Figures 2 and 3) is from a reciprocal-space refinement run. The correlation coefficient of the maps following refinement in this case is 0.85 (calculated using MAVE with a 5 Å protein mask). Note that we fitted the yeast molecular model into the cryo-EM map of the mammalian COPII cage. The sequences of *S. cerevisiae* and human Sec13 and Sec31 are 31% identical in the architectural core, and there are no major insertions or deletions in this region.

Supplemental Data

Supplemental Data include four figures and can be found with this article online at http://www.cell.com/cgi/content/full/129/7/1325/DC1/.

ACKNOWLEDGMENTS

We thank John Walker for assistance with data collection and reduction and Anand Saxena for use of synchrotron facilities at NSLS. This work was supported by grants from the NIH and the Howard Hughes Medical Institute (to J.G.), a fellowship from the Deutsche Forschungsgemeinschaft (to S.F.), and MSTP and NRSA fellowships (to J.D.M.).

Received: March 21, 2007
Revised: April 27, 2007
Accepted: May 11, 2007
Published: June 28, 2007

REFERENCES

Antonny, B. (2006). Membrane deformation by protein coats. Curr. Opin. Cell Biol. *18*, 386–394.

Antonny, B., Beraud-Dufour, S., Chardin, P., and Chabre, M. (1997). N-terminal hydrophobic residues of the G-protein ADP-ribosylation factor-1 insert into membrane phospholipids upon GDP to GTP exchange. Biochemistry *36*, 4675–4684.

Barlowe, C., Orci, L., Yeung, T., Hosobuchi, M., Hamamoto, S., Salama, N., Rexach, M.F., Ravazzola, M., Amherdt, M., and Schekman, R. (1994). COPII: a membrane coat formed by Sec proteins that drive vesicle budding from the endoplasmic reticulum. Cell *77*, 895–907.

Bi, X., Corpina, R.A., and Goldberg, J. (2002). Structure of the Sec23/24-Sar1 pre-budding complex of the COPII vesicle coat. Nature *419*, 271–277.

Bielli, A., Haney, C.J., Gabreski, G., Watkins, S.C., Bannykh, S.I., and Aridor, M. (2005). Regulation of Sar1 NH2 terminus by GTP binding and hydrolysis promotes membrane deformation to control COPII vesicle fission. J. Cell Biol. *171*, 919–924.

Bock, J.B., Matern, H.T., Peden, A.A., and Scheller, R.H. (2001). A genomic perspective on membrane compartment organization. Nature *409*, 839–841.

Bonifacino, J.S., and Glick, B.S. (2004). The mechanisms of vesicle budding and fusion. Cell *116*, 153–166.

Braell, W.A., Schlossman, D.M., Schmid, S.L., and Rothman, J.E. (1984). Dissociation of clathrin coats coupled to the hydrolysis of ATP: role of an uncoating ATPase. J. Cell Biol. *99*, 734–741.

Brünger, A.T. (1998). Crystallography and NMR system: A new software suite for macromolecular structure determination. Acta Crystallogr. D Biol. Crystallogr. *54*, 905–921.

CCP4. (1994). The CCP4 suite: programs for X-ray crystallography. Acta Crystallogr. D Biol. Crystallogr. *50*, 760–763.

Cheng, Y., Boll, W., Kirchhausen, T., Harrison, S.C., and Walz, T. (2007). Cryo-electron tomography of clathrin-coated vesicles: structural implications for coat assembly. J. Mol. Biol. *365*, 892–899.

Crowther, R.A., Finch, J.T., and Pearse, B.M. (1976). On the structure of coated vesicles. J. Mol. Biol. *103*, 785–798.

Devos, D., Dokudovskaya, S., Alber, F., Williams, R., Chait, B.T., Sali, A., and Rout, M.P. (2004). Components of coated vesicles and nuclear pore complexes share a common molecular architecture. PLoS Biol. *2*, 2085–2093. 10.1371/journal.pbio.0020380.

Dokudovskaya, S., Williams, R., Devos, D., Sali, A., Chait, B.T., and Rout, M.P. (2006). Protease accessibility laddering: A proteomic tool for probing protein structure. Structure *14*, 653–660.

Ehrlich, M., Boll, W., Van Oijen, A., Hariharan, R., Chandran, K., Nibert, M.L., and Kirchhausen, T. (2004). Endocytosis by random initiation and stabilization of clathrin-coated pits. Cell *118*, 591–605.

Fotin, A., Cheng, Y., Grigorieff, N., Walz, T., Harrison, S.C., and Kirchhausen, T. (2004a). Structure of an auxilin-bound clathrin coat and its implications for the mechanism of uncoating. Nature *432*, 649–653.

Fotin, A., Cheng, Y., Sliz, P., Grigorieff, N., Harrison, S.C., Kirchhausen, T., and Walz, T. (2004b). Molecular model for a complete clathrin lattice from electron cryomicroscopy. Nature *432*, 573–579.

Fromme, J.C., and Schekman, R. (2005). COPII-coated vesicles: flexible enough for large cargo? Curr. Opin. Cell Biol. *17*, 345–352.

Heuser, J.E. (1980). Three-dimensional visualization of coated vesicle formation in fibroblasts. J. Cell Biol. *84*, 560–583.

Jones, T.A., Zou, J.Y., Cowan, S.W., and Kjeldgaard, M. (1991). Improved methods for building protein models in electron density maps and the location of errors in these models. Acta Crystallogr. *A47*, 110–119.

Kajava, A.V. (2002). What curves α-solenoids? J. Biol. Chem. *277*, 49791–49798.

Kirchhausen, T. (2000). Three ways to make a vesicle. Nat. Rev. Mol. Cell Biol. *1*, 187–198.

Kleywegt, G.J., and Jones, T.A. (1999). Software for handling macromolecular envelopes. Acta Crystallogr. D Biol. Crystallogr. *55*, 941–944.

Lederkremer, G.Z., Cheng, Y., Petre, B.M., Vogan, E., Springer, S., Schekman, R., Walz, T., and Kirchhausen, T. (2001). Structure of the Sec23p/24p and Sec13p/31p complexes of COPII. Proc. Natl. Acad. Sci. USA *98*, 10704–10709.

Lee, M.C., Miller, E.A., Goldberg, J., Orci, L., and Schekman, R. (2004). Bi-directional protein transport between the ER and Golgi. Annu. Rev. Cell Dev. Biol. *20*, 87–123.

Lee, M.C., Orci, L., Hamamoto, S., Futai, E., Ravazzola, M., and Schekman, R. (2005). Sar1p N-terminal helix initiates membrane curvature and completes the fission of a COPII vesicle. Cell *122*, 605–617.

Matsuoka, K., Orci, L., Amherdt, M., Bednarek, S.Y., Hamamoto, S., Schekman, R., and Yeung, T. (1998). COPII-coated vesicle formation reconstituted with purified coat proteins and chemically defined liposomes. Cell *93*, 263–275.

Matsuoka, K., Schekman, R., Orci, L., and Heuser, J.E. (2001). Surface structure of the COPII-coated vesicle. Proc. Natl. Acad. Sci. USA *98*, 13705–13709.

Miller, E.A., Beilharz, T.H., Malkus, P.N., Lee, M.C., Hamamoto, S., Orci, L., and Schekman, R. (2003). Multiple cargo binding sites on the COPII subunit Se24p ensure capture of diverse membrane proteins into transport vesicles. Cell *114*, 497–509.

Mossessova, E., Bickford, L.C., and Goldberg, J. (2003). SNARE selectivity of the COPII coat. Cell *114*, 483–495.

Otwinowski, W., and Minor, W. (1997). Processing of X-ray diffraction data collected in oscillation mode. Methods Enzymol. *276*, 307–326.

Pearse, B.M., Smith, C.J., and Owen, D.J. (2000). Clathrin coat construction in endocytosis. Curr. Opin. Struct. Biol. *10*, 220–228.

Shaywitz, D.A., Espenshade, P.J., Gimeno, R.E., and Kaiser, C.A. (1997). COPII subunit interactions in the assembly of the vesicle coat. J. Biol. Chem. *272*, 25413–25416.

Shugrue, C.A., Kolen, E.R., Peters, H., Czernik, A., Kaiser, C., Matovcik, L., and Gorelick, F. (1999). Identification of the putative mammalian orthologue of Sec31P, a component of the COPII coat. J. Cell Sci. *112*, 4546–4556.

Stagg, S.M., Gürkan, C., Fowler, D.M., LaPointe, P., Foss, T.R., Potter, C.S., Carragher, B., and Balch, W.E. (2006). Structure of the Sec13/31 COPII coat cage. Nature *439*, 234–238.

Takamori, S., Holt, M., Stenius, K., Lemke, E.A., Gronborg, M., Riedel, D., Urlaub, H., Schenck, S., Brugger, B., Ringler, P., et al. (2006). Molecular anatomy of a trafficking organelle. Cell *127*, 831–846.

ter Haar, E., Musacchio, A., Harrison, S.C., and Kirchhausen, T. (1998). Atomic structure of clathrin: a beta propeller terminal domain joins an alpha zigzag linker. Cell *95*, 563–573.

Terwilliger, T.C., and Berendzen, J. (1999). Automated MAD and MIR structure solution. Acta Crystallogr. D Biol. Crystallogr. *55*, 849–861.

Ybe, J.A., Brodsky, F.M., Hofmann, K., Lin, K., Liu, S.H., Chen, L., Earnest, T.N., Fletterick, R.J., and Hwang, P.K. (1999). Clathrin self-assembly is mediated by a tandemly repeated superhelix. Nature *399*, 371–375.

Accession Numbers

The atomic coordinates have been deposited in the Protein Data Bank with the accession codes 2PM6, 2PM7, and 2PM9 (see Table 1).